The EMBO Journal (2009) 28, 3132–3144 | © 2009 European Molecular Biology Organization | All Rights Reserved 0261-4189/09
www.embojournal.org

THE EMBO JOURNAL

α-parvin controls vascular mural cell recruitment to vessel wall by regulating RhoA/ROCK signalling

Eloi Montanez, Sara A Wickström, Johannes Altstätter, Haiyan Chu and Reinhard Fässler*

Department of Molecular Medicine, Max Planck Institute of Biochemistry, Martinsried, Germany

During blood vessel development, vascular smooth muscle cells (vSMCs) and pericytes (PCs) are recruited to nascent vessels to stabilize them and to guide further vessel remodelling. Here, we show that loss of the focal adhesion (FA) protein α-parvin (α-pv) in mice leads to embryonic lethality due to severe cardiovascular defects. The vascular abnormalities are characterized by poor vessel remodelling, impaired coverage of endothelial tubes with vSMC/PCs and defective association of the recruited vSMC/PCs with endothelial cells (ECs). α-pv-deficient vSMCs are round and hypercontractile leading either to their accumulation in the tissue or to local vessel constrictions. Because of the high contractility, α-pv-deficient vSMCs fail to polarize their cytoskeleton resulting in loss of persistent and directed migration. Mechanistically, the absence of α-pv leads to increased RhoA and Rho-kinase (ROCK)-mediated signalling, activation of myosin II and actomyosin hypercontraction in vSMCs. Our findings show that α-pv represents an essential adhesion checkpoint that controls RhoA/ROCK-mediated contractility in vSMCs.

The EMBO Journal (2009) **28,** 3132–3144. doi:10.1038/emboj.2009.295; Published online 1 October 2009
Subject Categories: cell & tissue architecture; development
Keywords: angiogenesis; contractility; integrin; migration/parvin

Introduction

The cardiovascular system is the first functional organ that develops in vertebrate embryos. Vascular development starts with the differentiation and expansion of endothelial cell (EC) precursors that coalesce into a primitive vascular network. This vascular plexus is then extended and remodelled by a process called angiogenesis, which involves sprouting, branching and fusion (Risau, 1997). Once the ECs are assembled into vascular tubes, they become surrounded by mural cells (MCs) of the smooth muscle cell lineage, referred to as pericytes (PCs) and vascular smooth muscle cells (vSMCs). PCs are associated with capillaries, small venules and immature blood vessels in which they are enclosed by a single basement membrane (BM). In contrast, vSMCs are associated with mature and large blood vessels in which they form one or several sheets around the BM of ECs. The vSMC/PCs are essential for blood vessel development, as they provide mechanical support required to counterbalance the increasing blood pressure, control ECs proliferation, limit further sprouting and regulate the vascular tone with their highly contractile actomyosin cytoskeleton (Adams and Alitalo, 2007).

The vSMC/PCs differentiate from the mesenchyme and migrate around the growing blood vessels. The migration to and spreading on developing blood vessels are tightly regulated by growth factors and extracellular matrix (ECM) proteins, and their receptors such as integrins. Integrins are heterodimeric cell adhesion molecules composed of α and β subunits. When bound to the ECM they cluster and form focal adhesions (FAs), through which they relay signals into cells (Hynes, 2002; Legate *et al*, 2009). *In vitro* and *in vivo* studies have shown that integrin adhesion has essential functions in angiogenesis and vascular remodelling. For instance, deletion of the β1 integrin gene in ECs impairs angiogenesis (Carlson *et al*, 2008; Tanjore *et al*, 2008) and deletion in MCs impairs their ability to spread, differentiate and support vessel wall stability (Abraham *et al*, 2008). Conversely, ablation of genes encoding for integrin ligands such as fibronectin (FN), laminin α4 or collagen 4a1/2 has also a fatal effect on blood vessel formation (George *et al*, 1993; Thyboll *et al*, 2002; Pöschl *et al*, 2004). How integrins execute these properties is less clear.

The cytoplasmic domains of integrins are short and lack enzymatic activity, and therefore they trigger signalling by recruiting kinases such as FAK and src, and adaptor proteins such as integrin-linked kinase (ILK), PINCH and parvins. Parvins are a family of adaptor proteins consisting of three members; α-parvin/actopaxin/CH-ILKBP (α-pv), which is ubiquitously expressed; β-parvin/affixin (β-pv), which is enriched in heart and skeletal muscle; and γ-parvin (γ-pv) whose expression is restricted to haematopoietic cells (Nikolopoulos and Turner, 2000; Olski *et al*, 2001; Tu *et al*, 2001; Yamaji *et al*, 2001; Chu *et al*, 2006). Together with ILK and PINCH they form a ternary protein complex (IPP complex) that localizes to FAs. Parvins consist of an N-terminal polypeptide stretch followed by a single actin-binding domain (ABD) that consists of two in tandem arranged calponin homology (CH) domains. The ABD domain enables parvins to recruit F-actin to FAs and associate with stress fibres. Additional parvin-binding partners are actin binding and regulatory proteins including paxillin, Hic5, α-actinin, CdGAP and α-PIX, which explains the prominent functions of parvins in integrin-mediated adhesion and actin-dependent processes such as cell shape regulation and cell migration (Legate *et al*, 2006).

Vascular tone, which is regulated by the actomyosin-mediated contractility of the vSMCs, controls the blood

*Corresponding author. Department of Molecular Medicine, Max Planck Institute of Biochemistry, 82152 Martinsried, Germany.
Tel.: +49 89 8578 2072; Fax: +49 89 8578 2422;
E-mail: faessler@biochem.mpg.de

Received: 10 July 2009; accepted: 15 September 2009; published online: 1 October 2009

pressure and tissue perfusion. The contraction and relaxation of smooth muscle actin (SMA) filaments in vSMCs are controlled through phosphorylation of the myosin light chain (MLC). The phosphorylation of MLC is mediated by myosin light chain kinase (MLCK) and reversed by myosin light chain phosphatase (MLCP). Vasodilators activate MLCP, which causes MLC dephosphorylation and relaxation, whereas vasoconstrictors induce phosphorylation and inhibition of MLCP activity, which in turn stabilizes MLC phosphorylation and leads to contraction (Karnam, 2006). Vasoconstrictor agonists promote contractility of vSMCs through RhoA-mediated activation of ROCK, which in turn can either indirectly activate MLC through phosphorylation and inactivation of MLCP, or by directly phosphorylating MLC (Amano *et al*, 1996; Kimura *et al*, 1996). The parvin-binding partner ILK has also been shown to directly phosphorylate MLC and thereby modulate vSMC contraction (Wilson *et al*, 2005). A basal RhoA activity is required for cardiovascular homeostasis, whereas a sustained hyperactivation of RhoA is a common feature of several cardiovascular pathologies. Furthermore, RhoA signalling is also critical for cell polarity and directed cell migration (Danen *et al*, 2005) by promoting the maturation of integrin adhesion sites, formation of stress fibres and cell contraction at the rear (Xu *et al*, 2003). Therefore, a tight regulation of RhoA in vSMCs is crucial for the mature vascular system but may be equally important during the recruitment of vSMCs to developing vessels.

To directly address the function of α-pv *in vivo*, we generated mice and cells lacking α-pv expression. Our findings indicate that α-pv controls vSMC/PC recruitment to developing vessels and vessel wall stability by regulating RhoA/ROCK signalling in vSMCs.

Results

Loss of α-pv leads to severe cardiovascular defects

To explore the functions of α-pv *in vivo*, we disrupted the *α-pv* gene by homologous recombination in embryonic stem (ES) cells and generated α-pv mutant mice (Supplementary Figure 1A and B). Mice heterozygous for the α-pv null mutation (α-pv$^{+/-}$) were viable and phenotypically normal (data not shown). α-pv$^{+/-}$ intercrosses failed to yield newborn α-pv homozygous mutant (α-pv$^{-/-}$) mice. Timed mating of α-pv$^{+/-}$ intercrosses showed that α-pv$^{-/-}$ mice were present at the expected Mendelian ratio up to embryonic day (E) 11.5 (Supplementary Table 1). Lethality of α-pv$^{-/-}$ mice commenced at around E10.5 and no alive α-pv$^{-/-}$ mice were found later than E14.5 (Supplementary Table 1). Western blot analysis of E9.5 α-pv$^{-/-}$ embryo and yolk sac (YS) lysates showed loss of α-pv expression, unaltered or increased levels of β-pv and slightly decreased levels of ILK and PINCH1 when compared with wild-type (wt) lysates (Supplementary Figure 1C and D).

Development of α-pv$^{-/-}$ embryos was normal until E9.5 (data not shown). Growth retardation was first evident in E10.5 α-pv$^{-/-}$ embryos (Figure 1A). α-pv$^{-/-}$ embryos displayed different degrees of cardiovascular abnormalities including aberrant vascular beds with dilated blood vessels and pericardial effusion (Figure 1A and B; Supplementary Figure 2A). By E12.5, α-pv$^{-/-}$ embryos showed whole-body edema and severe bleedings due to vessel rupture (Figure 1A and B; Supplementary Figure 2B).

Aberrant cardiac morphogenesis and disrupted sarcomeric integrity in α-pv$^{-/-}$ embryos

To examine the heart abnormalities, we performed histological analysis of serial sections of wt and α-pv$^{-/-}$ embryonic hearts. Heart chambers developed normally in α-pv$^{-/-}$ embryos (data not shown). However, although E12.5 wt embryos showed septation of the truncus arteriosus resulting in an ascending aorta and pulmonary trunk (Figure 1C), α-pv$^{-/-}$ embryos showed a defective septation of the truncus arteriosus leading to a persistent single outflow tract (OFT) (Figure 1C).

Cell-ECM adhesion mediated by integrins is required to stabilize myofibrils (Fässler *et al*, 1996). Immunostaining of α-actinin and desmin, important Z-disc proteins that cross-link sarcomeric actin and connect Z-discs with adjacent myofibrils, showed reduced numbers of cardiomyofribrils in α-pv$^{-/-}$ embryos compared with wt littermates (Figure 1D and data not shown). Moreover, wt cardiomyocytes were elongated and aligned in a parallel manner, while α-pv$^{-/-}$ cardiomyocytes were round and distributed in a random pattern (Figure 1D). In line with earlier reports (Chen *et al*, 2005), we found that α-pv is localized at FAs as well as at Z-disc of the sarcomeres in normal cardiomyocytes (data not shown). Together, these data indicate that α-pv is required for the development of the OFT of the heart and for maintaining the structure and stability of sarcomeres, but not for initiating cardiomyofibrillogenesis. Because of the well-known functions of integrins, ILK and parvins for cardiac muscle morphogenesis and function (Fässler *et al*, 1996; Chen *et al*, 2005; Bendig *et al*, 2006), we focused our further analysis on the vascular defects.

Defective MC coverage in α-pv$^{-/-}$ embryos

To study the vascular abnormalities of α-pv$^{-/-}$ embryos in more detail, we performed whole mount immunostaining of wt and α-pv$^{-/-}$ embryos and YSs using antibodies against CD31, αSMA and anti-neuron glial 2 (NG2) to visualize ECs and MCs, respectively. Immunostaining for CD31 revealed the presence of a vascular plexus with microvessel and macrovessel containing blood cells in E10.5 and E11.5 α-pv$^{-/-}$ embryos and YSs (Figure 2A; Supplementary Figure 2C). In addition, isolated primary ECs from α-pv$^{-/-}$ YSs did not show differences in their ability to adhere and spread on collagen I (Col I) and FN (Supplementary Figure 2D and E and data not shown). Furthermore, ECs differentiated from α-pv$^{-/-}$ ES cells were able to migrate and form blood vessel-like structures comparable to wt ECs (Supplementary Figure 2F), suggesting that the vascular defects do not arise from defects in ECs.

However, α-pv$^{-/-}$ vessels were frequently enlarged and exhibited multiple microaneurysms, whereas in other areas they were constricted (Figure 2A–C; Supplementary Figure 3A). Vessel enlargement was associated with reduced MC coverage (Figure 2A; Supplementary Figure 3B). MCs directly interact with ECs and regulate vessel sprouting. Consistently with this function, the number of vascular sprouts was significantly increased in the vascular plexus of α-pv$^{-/-}$ embryos (Supplementary Figure 3C and D).

To assess the defect in MC coverage, we analysed the hindbrain vasculature, which is particularly rich in these cells (Abramsson *et al*, 2007). Quantitative analysis of EC coverage by PCs revealed that in wt embryos, the PCs were

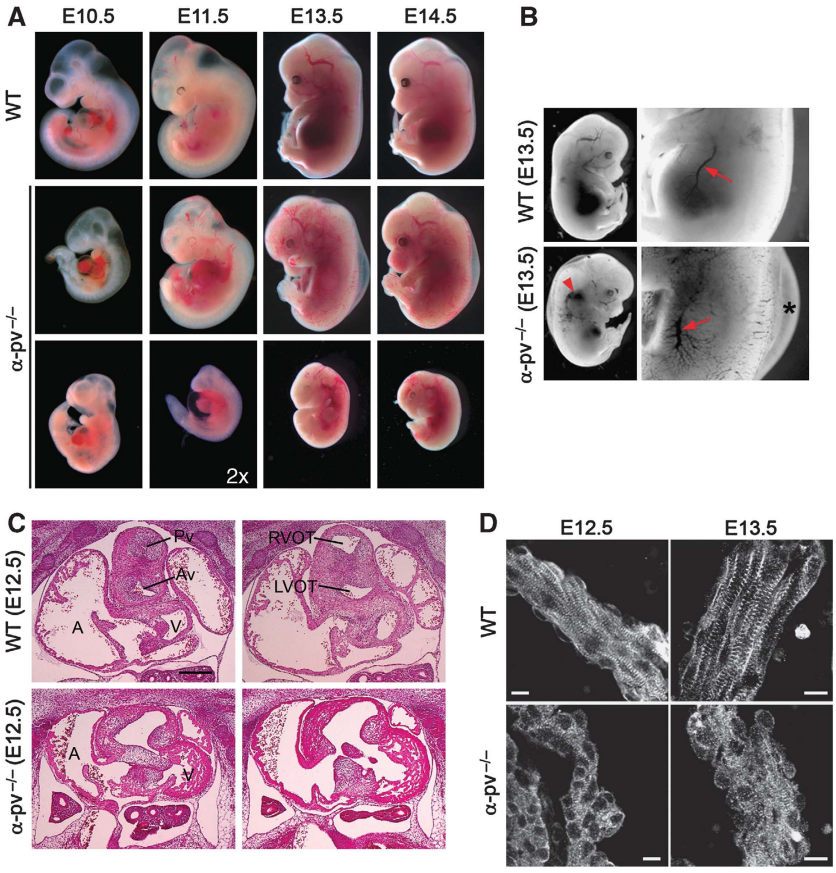

Figure 1 Embryonic lethality and cardiovascular defects in the absence of α-pv expression. (**A**) Gross examination of wt and α-pv$^{-/-}$ embryos. (**B**) α-pv$^{-/-}$ embryos display bleedings (arrowhead), whole-body edema (asterisks) and enlarged vessels (arrows). (**C**) Hematoxylin and eosin staining of frontal sections through the heart outflow tract (OFT) of E12.5 wt and α-pv$^{-/-}$ embryos. Bar: 50 μm. (**D**) Confocal sections of E12.5-13.5 hearts from wt and α-pv$^{-/-}$ embryos. Cardiomyocytes were labelled with α-actinin. Bar: 10 μm. A, atrium; V, ventricle; Av, aortic valve; Pv, pulmonary valve; RVOT, right ventricular OFT; LVOT, left ventricular OFT.

tightly associated with ECs and the relative proportion of endothelial staining (CD31) overlapping with PC staining (NG2) per total vessel area was 58% (±9.6) (Figure 2D and E). In contrast, the PCs of α-pv$^{-/-}$ embryos frequently stretched away from the endothelium, and covered only 23% (±2.4) of the endothelial area (Figure 2D and E). Furthermore, analysis of the distance from the growing endothelial edge to the closest PCs revealed that in E10.5 wt embryos, the PCs arrived to the growing front of the vascular plexus marked by the tip cells, whereas in α-pv$^{-/-}$ littermates PCs failed to reach the growing vascular front (Figure 2F). No differences could be detected in E11.5 embryos, indicating that lack of α-pv is a result of a delay in PC recruitment *in vivo* (Figure 2F). Poor MC coverage and impaired MC/EC association were also observed in blood vessels of α-pv$^{-/-}$ YSs and placentas (Supplementary Figure 4A and B). Collectively, these results indicate that α-pv is dispensable for vasculogenesis, but required for vascular maturation and MC investment into vessel walls.

α-pv regulates spreading and polarity of MCs

Successful MC coverage of the vascular bed depends on a number of factors including proliferation, survival, spreading and migration (Beck and D'Amore, 1997). We found no apparent defects in MC proliferation or increased apoptosis of E9.5, E10.5, E11.5 and E12.5 α-pv$^{-/-}$ embryos (Supplementary Figure 5 and data not shown). However, in contrast to wt vSMCs/PCs, which spread and showed strong and often punctate αSMA staining at the plasma membrane and thin filamentous staining in the cytoplasm (Figure 3A and B), α-pv$^{-/-}$ vSMC/PCs displayed a round shape and showed thick αSMA-positive actin bundles traversing the cytoplasm in a criss-cross manner (Figure 3A and B; Supplementary Figure 6).

To analyse this defect in more detail, we isolated SMA-positive cells from wt and α-pv$^{-/-}$ YSs and tested their ability to adhere and spread on ECM proteins. No difference in the ability of wt and α-pv$^{-/-}$ cells to adhere to laminin-111 (LN111), FN or Col I was observed (Figure 3C). In addition, the cell surface expression pattern of integrins was also unaltered (data not shown). However, despite their ability to adhere to ECM substrates, α-pv$^{-/-}$ cells remained round even after an overnight culture and developed multiple membrane protrusions, whereas wt cells spread within 60 min after plating (Figure 3D and E). Live video microscopy showed that wt cells were able to extend lamellipodia and spread to adopt a flattened shape. In contrast, α-pv$^{-/-}$ cells displayed continuous, highly dynamic and instable membrane ruffling at the cell cortex, leading to the formation of multiple retraction fibres (Supplementary Movies 1 and 2). To further analyse the morphology of the cells, we performed computational analysis of the cell shape (shape factor;

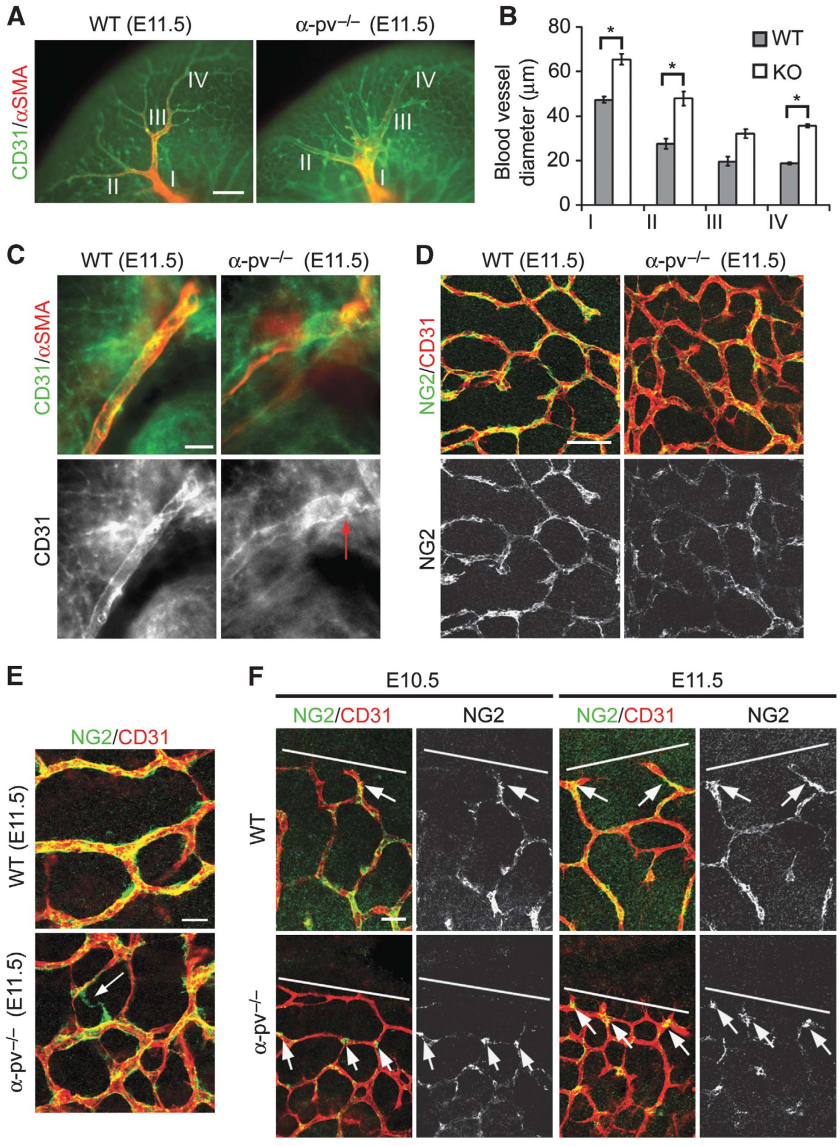

Figure 2 Reduced MC coverage and defective MC/EC association in the absence of α-pv$^{-/-}$. (**A**) Whole mount immunostaining of the head vasculature. ECs were labelled with CD31 (green) and vSMC with αSMA (red). Bar: 0.2 mm. (**B**) Quantification of the diameter of the macrovessels (I) and microvessel (II, III, IV) from the head vasculature. Values are mean ± s.e.m.; *$P = 0.012$ (I); *$P = 0.039$ (II); $P = 0.091$ (III); *$P = 0.01$ (IV). (**C**) CD31 and αSMA whole mount immunostaining of the right subclavian artery. Note the defective vSMC coverage and the presence of local constriction (red arrows) of α-pv$^{-/-}$ vasculature. Bar: 50 μm. (D–F) Whole mount immunostaining of E10.5-115 hindbrain endothelium CD31 (red) and associated PCs (green) from wt and α-pv$^{-/-}$ embryos. Bar: 50 μm (D) and 20 μm (E, F). (**D**) Reduced MC coverage in the peripheral region of the hindbrain of α-pv$^{-/-}$ embryos. (**E**) Defective MC/EC association in α-pv$^{-/-}$ vasculature (arrow). (**F**) Delayed PC recruitment in α-pv$^{-/-}$ embryos. The distance of the endothelial edge (line) to the closest PC (arrows) is labelled.

described in detail in Materials and methods), of individual cells plated for 3 h on FN. We found that >90% of the wt cells reached a shape factor value between 0.25 and 0.75, indicating that they contain a single broad lamella (Figure 3F). In contrast, more than half of the α-pv$^{-/-}$ cells adopted a value below 0.25, which corresponds to an unpolarized cell with either an elongated or a highly complex outline of the plasma membrane (Figure 3F). Importantly, the spreading and shape defects were rescued by re-expressing α-pv-GFP in α-pv$^{-/-}$ SMA-positive cells (Figure 3G–I).

Sustained cell contraction leads to retraction, followed by cell rounding and formation of retraction fibres, which are, unlike stress fibres, not associated with myosin (M) (Cramer and Mitchison, 1995). To examine whether cell spreading, shape and polarity defects of the α-pv$^{-/-}$ cells were a consequence of abnormal cell contraction, we performed double immunostaining of wt and α-pv$^{-/-}$ cells using anti-αSMA and anti-M-II antibodies and found that the actin protrusions of α-pv$^{-/-}$ cells lacked M-II (Figure 4A). The majority of the M-II signal was observed in the thick cortical actin bundles of the α-pv$^{-/-}$ cells, whereas stress fibres were positive in wt cells (Figure 4A). These data further indicate that the actin protrusions of α-pv$^{-/-}$ cells are retraction fibres.

α-pv controls RhoA/ROCK-mediated cell contraction

The morphological analysis suggested that the α-pv$^{-/-}$ SMA-positive cells were highly contractile. Sustained contraction

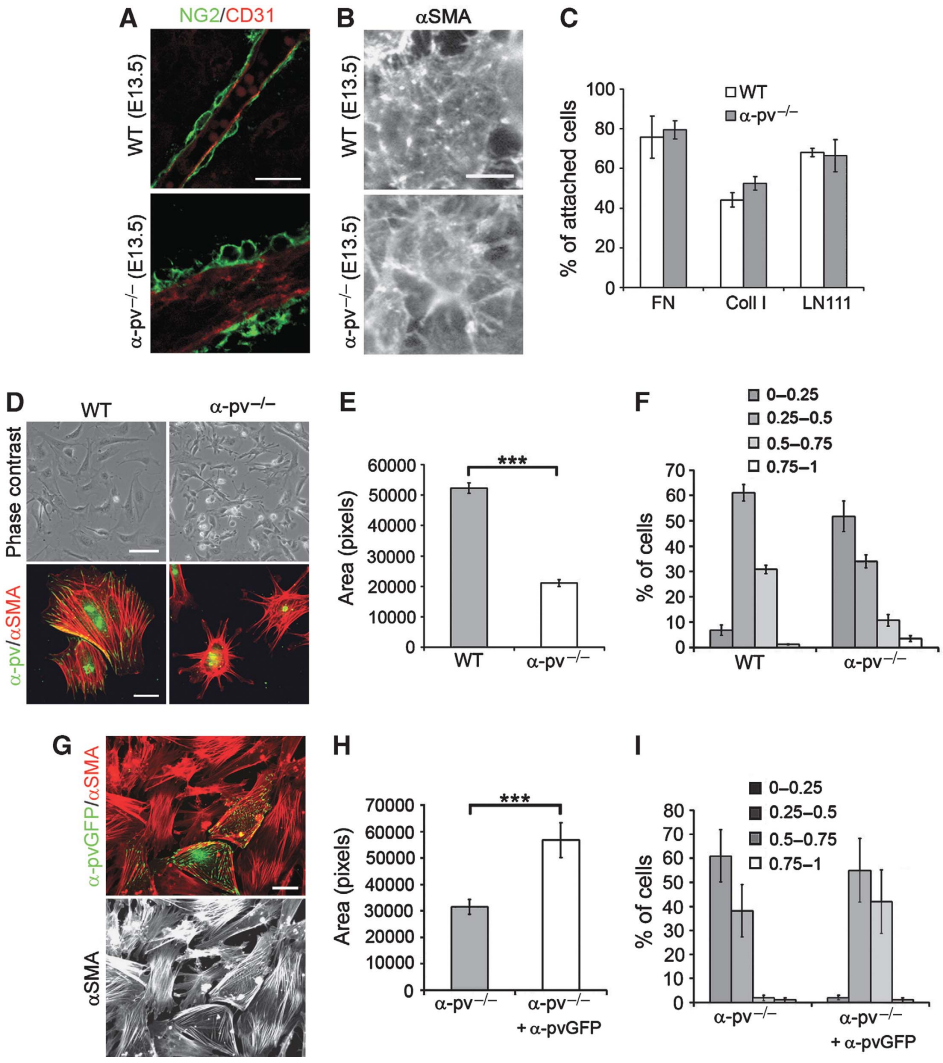

Figure 3 Impaired cell spreading and cell shape of MCs in the absence of α-pv$^{-/-}$. (**A**) Whole mount immunostaining of vasculature of E13.5 YSs. ECs were labelled with CD31 and MCs with NG2. Bar: 20 μm. (**B**) Whole mount immunostaining of vasculature of E13.5 YSs. MCs were labelled with αSMA. Bar: 10 μm. (**C**) Adhesion assay of isolated wt and α-pv$^{-/-}$ SMA-positive cells on different ECM substrates. Values are mean ± s.e.m. (**D**) Brightfield images and immunofluorescence staining for αSMA (red) and α-pv (green) of wt and α-pv $^{-/-}$ SMA-positive cells seeded of FN (10 μg/ml). Bar: 50 and 10 μm, respectively. (**E**) Quantification of cell area and (**F**) shape factor of wt and α-pv$^{-/-}$ SMA-positive cells. Values are mean ± s.e.m; ***$P = 0.0001$ (**G–I**) Re-expression of α-pv-GFP restores size and shape of α-pv$^{-/-}$ SMA-positive cells. Green represents the EGFP signal and the cytoskeleton is visualized with αSMA (red). Bar: 20 μm. Values are mean ± s.e.m; ***$P = 0.0001$.

of vSMCs can be mediated by the RhoA/ROCK/MLC2 signalling pathway (Karnam, 2006). To determine RhoA activity in primary vSMCs, we measured Rho-GTP binding to the Rhotekin-Rho binding domain and found a significant increase in RhoA-GTP levels in primary α-pv$^{-/-}$ cells (Figure 4B). Consistent with the increased RhoA activity, α-pv$^{-/-}$ cells showed higher levels of phospho-MLC2 than wt cells (Figure 4C). Increased levels of RhoA-GTP and elevated levels of phospho-MLC2 were also observed in immortalized SMA-positive cells derived from E9.5 α-pv$^{-/-}$ embryos (Figure 4D and E; Supplementary Figure 7A and B). Re-expression of α-pv in the immortalized cells induced normal cell spreading, accompanied by loss of retraction fibres and reduced RhoA-GTP and phospho-MLC2 levels (Figure 4D and E; Supplementary Figure 7A–D). Importantly, immunostaining of tissue sections of YSs also revealed elevated MLC2 phosphorylation in vSMC/PCs in the vascular plexus of E13.5 α-pv$^{-/-}$ embryos (Figure 4F), indicating that activation of the RhoA/ROCK/MLC2 signalling pathway is also elevated *in vivo*.

To test whether increased RhoA and MLC2 activity leads to increased contractile properties of vSMCs, we seeded wt or α-pv$^{-/-}$ cells in 3D collagen gels and observed gel contraction over a time period of 48 h. Indeed, α-pv$^{-/-}$ cells showed a two-fold increase in gel contraction compared with wt cells (Figure 5A and B).

Consistent with increased RhoA/ROCK signalling, addition of Y-27632, an inhibitor of ROCK, to collagen gels normalized the collagen gel contraction (Figure 5B). Interestingly, treatment of α-pv$^{-/-}$ cells with ML-9, an inhibitor of MLCK, did not change the contractile properties of α-pv$^{-/-}$ cells (data not shown). Finally, when cells were cultured in the presence of Y-27632, wt and α-pv$^{-/-}$ cells displayed similar morphology (Figure 5C and D). Collectively, these results indicate that α-pv controls vSMC contraction through negatively regulating the RhoA/ROCK/MLC2 signalling pathway.

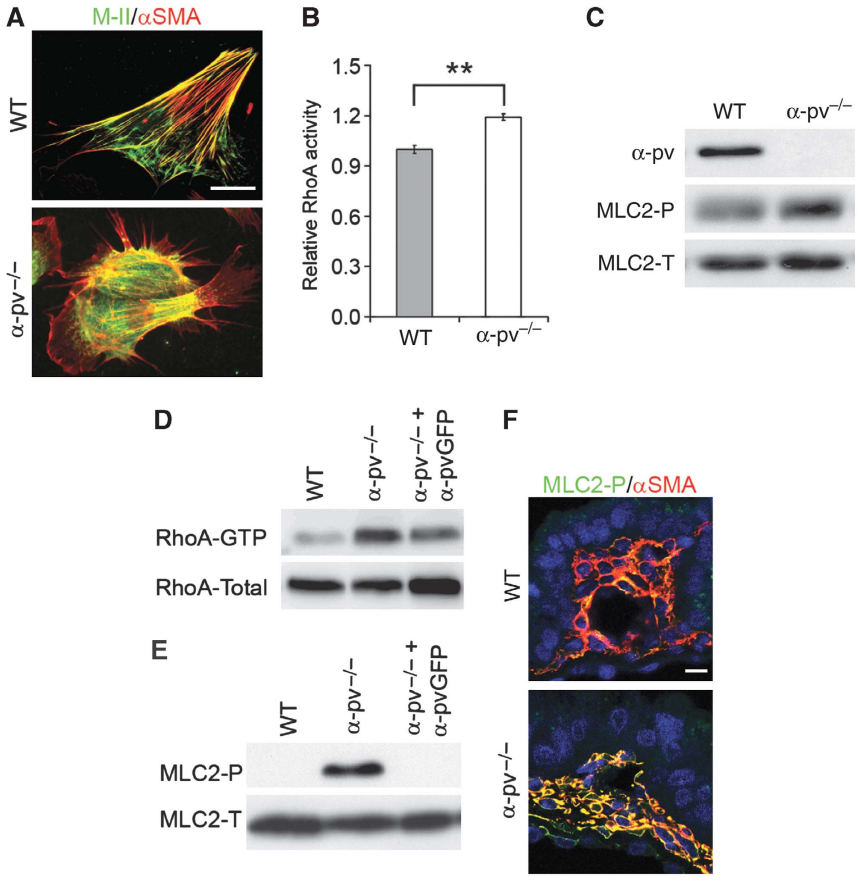

Figure 4 Elevated RhoA activity in the absence of α-pv. (**A**) Immunofluorescence staining for αSMA (red) and M-II (green) of wt and α-pv$^{-/-}$ SMA-positive cells. Note that actin protrusions of α-pv$^{-/-}$ cells lack M-II staining. Bar: 25 μm. Freshly isolated α-pv$^{-/-}$ SMA-positive cells show increased RhoA activity. Values are mean +/− s.e.m.; $^{**}P = 0.0012$ (**B**) and increased phosphorylation of MLC2 (**C**). Total MLC2 served as loading control. Immortalized α-pv$^{-/-}$ SMA-positive cells show increased RhoA activity (**D**) and increased phosphorylation of MLC2 (**E**). (**F**) Immunofluorescence analysis of E13.5 YS sections with αSMA (red) and phospho-MLC2 (green) shows increased phosphorylation of MLC2 *in vivo*. Bar: 20 μm.

α-pv controls MC recruitment and directed cell migration

MC recruitment to angiogenic vessels depends on platelet-derived growth factor BB (PDGF-BB)-mediated directed migration (Hellström *et al*, 1999; Abramsson *et al*, 2007). As we observed defects in this process, we next determined whether α-pv$^{-/-}$ SMA-positive cells were able to respond to PDGF-BB. To this end, we stimulated serum-starved primary wt and α-pv$^{-/-}$ cells with 100 ng/ml PDGF-BB and measured the phosphorylation levels of downstream signalling molecules. PDGF-BB treatment triggered a comparable increase in Erk and Akt phosphorylation in wt and α-pv$^{-/-}$ cells, indicating that loss of α-pv did not impair PDGFR signalling *per se* (Figure 6A and data not shown). To test whether α-pv$^{-/-}$ cells were still capable of migrating towards a source of PDGF-BB, we performed both chemokinesis and chemotaxis assays using Transwell motility chambers and found that α-pv$^{-/-}$ cells exhibited accelerated rates of random chemokinetic migration, but migrated less efficiently towards a PDGF-BB gradient compared with wt cells (Figure 6B and C). Similar results were observed in cells migrating to a source of serum (data not shown). These data indicate that α-pv is required for persistent directed migration.

Cell polarity is essential for directed migration. Live video microscopy over a period of 12 h showed that wt cells extended stable lamellipodia in the direction of the movement, while α-pv$^{-/-}$ cells continuously formed lamellipodia-like protrusions that were highly instable and appeared randomly at different parts of the cells, causing continuous changes in the direction of cell movement (Supplementary Movies 3 and 4). Similar migration behaviour was observed in the immortalized cells, whereas re-expression of α-pv restored normal cell motility (Supplementary Movies 5, 6 and 7). Tracking of individual cells combined with statistical analysis confirmed that α-pv$^{-/-}$ cells moved significantly less persistently than wt cells (Figure 6D). In the presence of Y-27632, α-pv$^{-/-}$ cells formed stable lamellipodia, and the persistence of cell motility was restored to the level of wt cells (Figure 6D; Supplementary Movies 8 and 9).

Rac activity is essential for the establishment of lamellipodia and directed cell migration. It has been shown that α-pv can regulate Rac activity in HeLa and osteosarcoma cells by controlling the activity of the Rac/Cdc42 GAP CdGAP (LaLonde *et al*, 2006). To assess whether dysregulation of Rac activity is also involved in the altered lamellipodial dynamics of α-pv$^{-/-}$ SMA-positive cells, we determined Rac activity in immortalized cells during the first 90 min of spreading on FN. Adhesion to FN induced a transient increase in Rac-GTP levels that peaked after 10 min of spreading and was comparable in wt and α-pv$^{-/-}$ cells (Supplementary

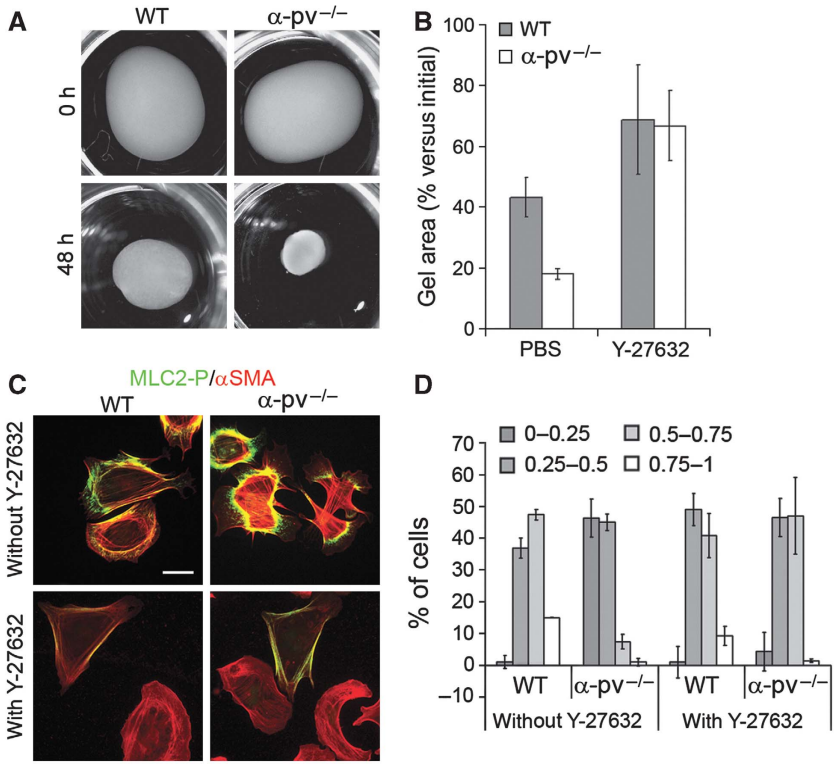

Figure 5 Increased collagen matrix contraction in the absence of α-pv. (**A**) Three-dimensional collagen gel containing wt and α-pv$^{-/-}$ SMA-positive cells. (**B**) Quantification of collagen gel area. α-pv$^{-/-}$ SMA-positive cells display higher collagen matrix contraction capacity than wt cells. Note that in the presence of ROCK inhibitor Y-27632 (1.5 μM) wt and α-pv$^{-/-}$ cells show similar contraction capacity. (**C**) Wt and α-pv$^{-/-}$ SMA-positive cells seeded on FN for 15 min in the absence and presence of Y-27632 (1.5 μM) and stained with αSMA (red) and phospho-MLC2 (green). Bar: 25 μm. (**D**) Quantification of shape factor of wt and α-pv$^{-/-}$ SMA-positive cells in the absence and presence of Y-27632. Values are mean ± s.e.m.

Figure 7E and F). Although in wt cells Rac-GTP levels remained stable for 30 min and gradually decreased to basal levels after 90 min of spreading, α-pv$^{-/-}$ cells showed a rapid decrease in Rac-GTP levels to baseline levels already after 10 min (Supplementary Figure 7E and F). The early decrease of Rac-GTP levels in α-pv$^{-/-}$ cells correlated with a strong increase in RhoA activity at this time point (Supplementary Figure 7G and H). Moreover, Y-27632-mediated inhibition of ROCK normalized Rac activity in α-pv$^{-/-}$ cells (Supplementary Figure 7I). These results indicate that Rac activation occurs normally in α-pv$^{-/-}$ cells, but its sustained activation is suppressed through elevated RhoA/ROCK activity.

α-pv-mediated regulation of RhoA is specific to MCs and is not compensated by β-pv

The interaction of parvins with ILK is necessary to target both proteins to FAs and to prevent degradation of the IPP complex (Legate *et al*, 2006). As the IPP complex is an important regulator of cell shape and cell migration, we tested whether loss of α-pv affects the stability and subcellular localization of the other members of the complex. WB analysis revealed normal levels of ILK and PINCH1 in α-pv$^{-/-}$ SMA-positive cells, whereas the levels of β-pv were increased when compared with wt cells (Figure 7A). Immunostaining showed normal ILK localization in FAs (Figure 7B). In addition, immunoprecipitation experiments from wt and α-pv$^{-/-}$ cells showed that ILK co-precipitated with β-pv both in the presence and absence of α-pv (Figure 7C). Furthermore, in wt cells both α- and β-pv associated with ILK, but not with each other (Figure 7C).

To assess whether the function of α-pv in regulating cell contractility is specific for vSMCs, we isolated and investigated wt and α-pv$^{-/-}$ fibroblasts (Supplementary Figure 8A). Like ECs, fibroblast lacking α-pv did not show apparent defects in spreading and actin cytoskeleton organization. In addition, there was no apparent difference in the levels of MLC2 phosphorylation in these cells (Supplementary Figure 8B and data not shown).

It has been suggested that ILK modulates vSMC contractility by directly phosphorylating MLC (Wilson *et al*, 2005). To test whether loss of α-pv could lead to hyperphosphorylation of MLC through ILK, we depleted ILK in wt cells using siRNA and found increased levels of MLC2 phosphorylation and reduced levels of α-pv (Figure 7D). To further confirm that the elevated RhoA/ROCK signalling was due to the loss of α-pv and not due to an upregulation of β-pv, we depleted β-pv in wt and α-pv$^{-/-}$ cells. Depletion of β-pv had no effect on MLC2 phosphorylation (Figure 7E), whereas depletion of α-pv in wt cells increased the levels of MLC2 phosphorylation (Figure 7F). Together, these data suggest that (i) β-pv can stabilize ILK and PINCH1 protein levels and localize them into FAs in the absence of α-pv, (ii) α- and β-pv exist in separate complexes containing ILK, (iii) the spreading and shape defects are exclusively due to the absence of α-pv and (iv) the ILK/α-pv complex is a negative regulator of MLC2 phosphorylation in these cells.

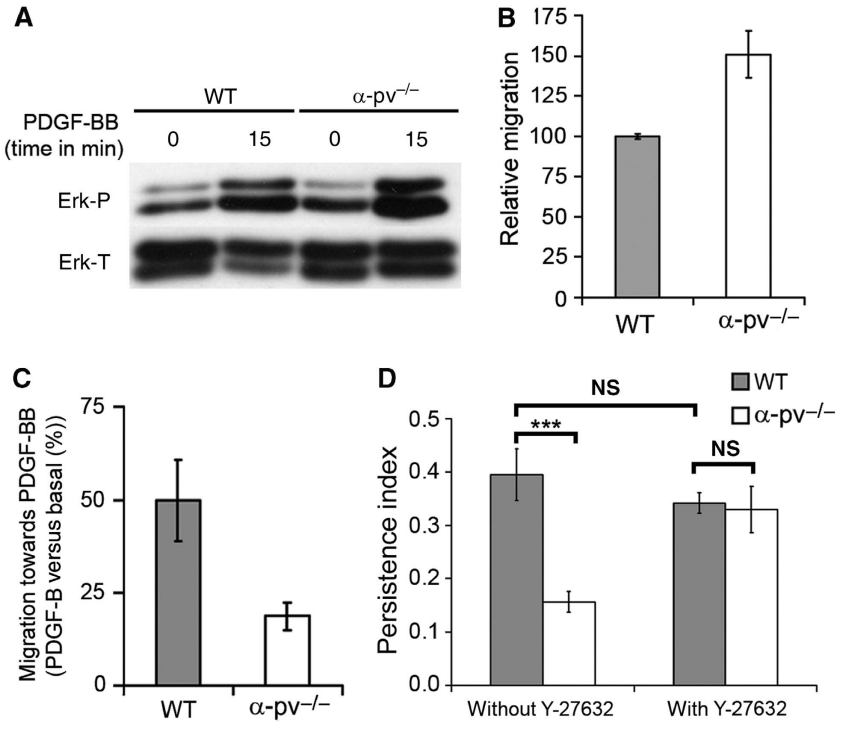

Figure 6 Normal PDGF-BB signalling but impaired directed cell migration of α-pv$^{-/-}$ SMA-positive cells. (**A**) Wt and α-pv$^{-/-}$ SMA-positive cells stimulated for 15 min with 100 ng/ml PDGF-BB show similar phosphorylation of Erk. Total Erk served as loading control. (**B**) Quantification of chemokinetic migration. Note that α-pv$^{-/-}$ cells display higher rates of random migration compared with wt cells. (**C**) Quantification of chemotactic migration using 20 ng/ml PDGF-BB as chemoattractant (24 h). Control medium without PDGF-BB was used to assess baseline migration. Note that although all cells migrated towards PDGF-BB, the ratio of stimulated/unstimulated migration is reduced in α-pv$^{-/-}$ cells. (**D**) Quantification of persistent motility of wt and α-pv$^{-/-}$ vSMCs (12 h) seeded on FN. Note that α-pv$^{-/-}$ cells move less persistently than wt cells, whereas in the presence of Y-27632 (0.5 μM), wt and cells display similar persistent motility. Values are mean ± s.e.m; ***$P = 0.0001$; NS, not significant.

Discussion

The results of our study show that α-pv is a central regulator of vascular maturation and blood vessel stability. Disruption of the α-pv gene in mice results in embryonic lethality due to severe cardiovascular defects. In the absence of α-pv, vascular beds are aberrantly organized and abnormally covered by MCs. α-pv$^{-/-}$ vSMCs display defects in cell spreading, polarity and directed migration. These cellular defects are caused by increased RhoA/ROCK activity that leads to elevated MLC2 phosphorylation and aberrant cell contractility.

The pump function of the heart has a critical role in embryonic development, growth and survival by transporting oxygen and nutrients through the vascular network and by promoting organogenesis such as vascular remodelling and formation of haematopoietic stem cells (Lucitti *et al*, 2007; Adamo *et al*, 2009; North *et al*, 2009). Therefore, severely impaired heart function caused either by defects during heart morphogenesis or by abnormal cardiomyocyte organization and sarcomere assembly can lead to embryonic lethality as early as E10.5-12.5 (Huang *et al*, 2003). Integrin-mediated cell adhesion has an essential function during cardiac development (Sengbusch *et al*, 2002). In this study, we report that α-pv is required for the remodelling of the OFT and formation and/or stability of cardiomyofribrils, which likely contributes to the early embryonic lethality of the α-pv$^{-/-}$ mice. These observations are in line with earlier studies reporting that β1 integrins, ILK and parvins have an essential function in heart development, cardiomyocyte contraction and integrity in different model organisms (Fässler *et al*, 1996; Chen *et al*, 2005; Bendig *et al*, 2006).

Deletion of α-pv also leads to severe vascular defects, including impaired vascular remodelling, vessel dilatation, formation of microaneurysms and vessel rupture. As cell type-specific ablation of the ILK gene in mice revealed an important function for ILK in vascular development and EC survival (Friedrich *et al*, 2004), it was important to determine whether α-pv would act in co-operation with ILK to regulate the endothelium. Interestingly, we found no increase in apoptosis of α-pv$^{-/-}$ ECs. Furthermore, α-pv$^{-/-}$ ECs adhere, spread and are able to migrate and form vascular networks comparable to wt ECs. This suggests that the defects in the vascular endothelium of α-pv$^{-/-}$ embryos are likely cell non-autonomous and arise from cells that regulate vascular remodelling and stability. In line with this hypothesis, we observed vascular abnormalities already in E10.5 embryos, a developmental stage when flow-dependent remodelling defects are still of minor importance. Although this observation indicates that vascular abnormalities develop independent of the heart defect, we need to determine the contribution of the defective heart function on the abnormal vascular remodelling (Lucitti *et al*, 2007) at later developmental stages by deleting the α-pv gene exclusively in cardiomyocytes using the Cre/loxP system. To this end, we have generated α-pv floxed mice.

Functional blood vessels consist of endothelial tubes surrounded by tightly associated and organized vSMC/PCs that provide stability to vessels. Dysfunction of vSMC/PCs is

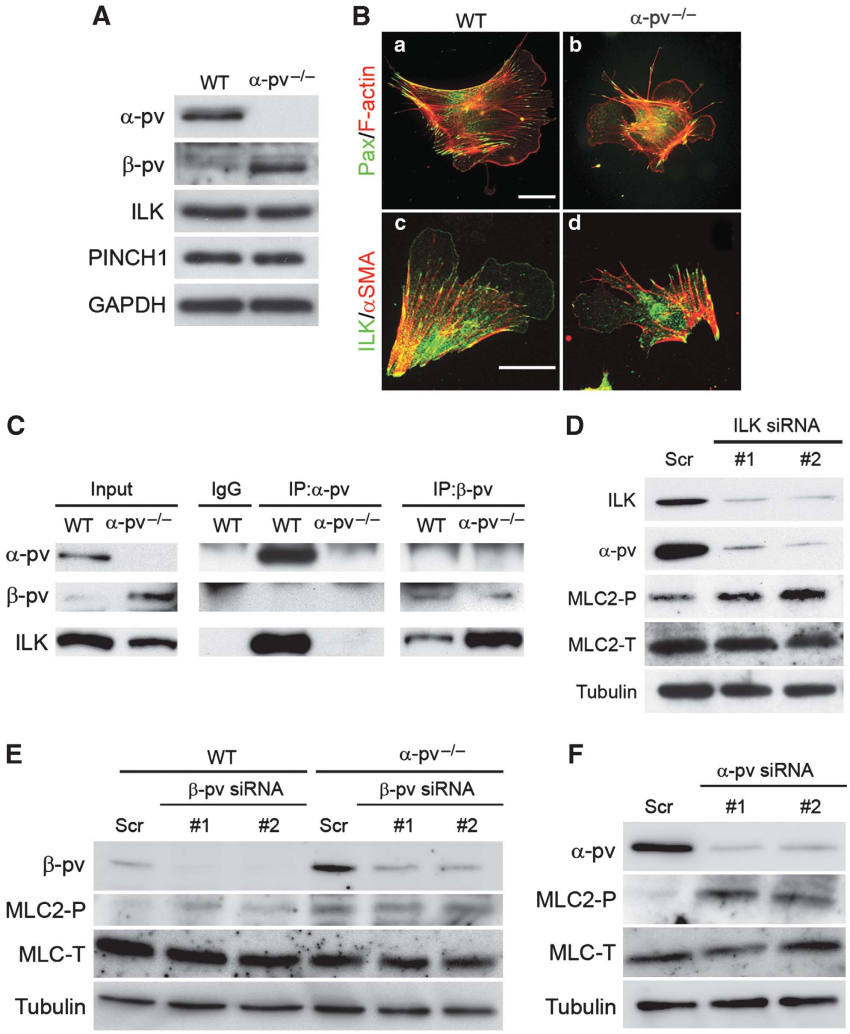

Figure 7 ILK/α-pv complex is a negative regulator of MC contractility. (**A**) Western blot analysis of IPP proteins in wt and α-pv$^{-/-}$ SMA-positive cells. Note that α-pv$^{-/-}$ cells show similar protein levels of ILK and PINCH1, and increased protein levels of β-pv compared with wt. (**B**) Immunofluorescence staining for paxillin (green) and F-actin (red) (a, b) and ILK (green) and αSMA (red) (c, d) of wt and α-pv$^{-/-}$ SMA-positive cells seeded of FN. Bar: 25 μm. (**C**) Immunoprecipitation experiments from wt and α-pv$^{-/-}$ SMA-positive cells. Note that both α- and β-pv co-immunoprecipitate with ILK but not with each other. (**D**) ILK depletion by two siRNA duplexes in wt cells induces increased MLC2 phosphorylation accompanied by reduced levels of α-pv. (**E**) β-pv depletion by two siRNA duplexes in wt and α-pv$^{-/-}$ cells does not change the levels of MLC2 phosphorylation. (**F**) α-pv depletion by two siRNA duplexes in wt cells induces increased MLC2 phosphorylation.

associated with dilated vessels, formation of microaneurysms and vessel wall disruption (Hellström *et al*, 2001; Boucher *et al*, 2003). The same defects were also observed in α-pv$^{-/-}$ embryos. Consistently, the endothelial tubes of α-pv$^{-/-}$ embryos are poorly covered with vSMC/PCs, and the few recruited cells fail to properly spread around the endothelial tube. To surround and stabilize the vascular endothelium, MCs have to proliferate and migrate to vessels. Integrin-mediated adhesion has an important function in both of these functions. This was shown by deleting the β1 integrin gene in MCs, which leads to aberrant proliferation of these cells and deficient vessel wall stability (Abraham *et al*, 2008), and by ablating the α4 integrin subunit, which impairs migration of vSMCs/PCs to developing blood vessels (Grazioli *et al*, 2006). We found no requirement of α-pv for proliferation or survival of vSMC/PCs indicating that the poor vSMC/PCs investment is not caused by a deficiency of vSMC/PCs. This finding also suggests that β1 integrin function is not completely compromised in the absence of α-pv, a notion further supported by the findings that α-pv$^{-/-}$ cells adhere normally to various ECM substrates and that ILK is normally recruited to integrin adhesion sites. Moreover, the restricted phenotype of the α-pv$^{-/-}$ mice to the cardiovascular system indicates that α-pv is indispensable for only a specific subset of signals downstream of β1 integrin.

Cell migration is directed by gradients of chemoattractants and/or repulsive molecules as well as by ECM molecules that serve as haptotactic tracks. During vascular development, MCs are attracted by a gradient of PDGF-BB produced by ECs to migrate directionally towards newly formed vessels (Hellström *et al*, 1999; Abramsson *et al*, 2007). Our results show that α-pv$^{-/-}$ MCs are improperly recruited to the vascular endothelium and that α-pv$^{-/-}$ vSMC-like cells display accelerated random motility but migrate less efficiently towards PDGF-BB or towards a serum source. Interestingly, α-pv$^{-/-}$ vSMCs are still capable of responding to PDGF-BB stimulation by activating mitogenic signalling pathways. These findings suggest that α-pv does not control recruitment

of MCs through regulating PDGFR signalling *per se*, but rather by regulating the molecular machinery required for efficient directional motility of MCs.

In response to a pro-migratory stimulus, cells polarize in the direction of the chemotactic gradient by extending a lamellipodium at the leading edge. Integrin-mediated adhesions then form directly behind the lamellipodium to stabilize the lamella and to exert a force between the ECM and the cytoskeleton required for the advance of the leading edge. To move the cell body forward, adhesions are subsequently disassembled at the cell rear, which is then pulled in the direction of motility by the contractile machinery of the actomyosin network (Ridley *et al*, 2003). Integrins and Rac establish a positive feedback loop within the leading edge that forms and maintains the lamella, whereas RhoA is necessary for the generation of contractile forces and tail retraction (Burridge and Wennerberg, 2004). Our results show that α-pv$^{-/-}$ vSMC fail to spread due to enhanced RhoA/ROCK activity leading to elevated MLC2 phosphorylation and increased cell contractility. This finding is consistent with earlier observations showing that cell spreading requires a transient downregulation of RhoA activity (Ren *et al*, 1999). Suppression of RhoA activity is necessary to promote lamellipodial protrusion during migration (Arthur *et al*, 2000; Arthur and Burridge, 2001). This is partly achieved by negative regulation of RhoA activity by Rac, which is transiently activated on cell adhesion to induce lamellipodia formation (Sander *et al*, 1999; del Pozo *et al*, 2000). On the other hand, RhoA activation restricts lamellae formation by inhibiting Rac activity (Tsuji *et al*, 2002; Worthylake and Burridge, 2003). We could also show that α-pv is not required for Rac activation induced by cell adhesion in vSMC-like cells. However, Rac activity is rapidly suppressed during the spreading of α-pv$^{-/-}$ SMA-positive cells. This downregulation occurs concomitantly with a robust upregulation of RhoA activity. These observations together with the finding that defects in cell spreading and in directional motility can be rescued with ROCK inhibitors and that the ROCK-inhibited cells are able to establish lamellipodia and normalize their Rac activity strongly suggests that the aberrant RhoA activity is the primary defect in α-pv$^{-/-}$ SMA-positive cells. ROCK-mediated activation of MLC2, which is located both at the leading edge and at the rear of the cell, leads to a global contraction of the cells and loss of cell polarity (Matsumura and Hartsthorne, 2008). Thus, as a consequence of the elevated RhoA activity and the subsequent suppression of Rac activity, α-pv$^{-/-}$ vSMC are not able to properly establish a stable leading edge and a cell rear, resulting in highly inefficient and non-directional cell motility.

The mechanisms by which integrin adhesion regulates RhoA activity are complex, and it seems that distinct integrin heterodimers use different strategies to regulate this activity, even in response to the same extracellular ligand (Danen *et al*, 2005). The parvin-binding partner ILK has been shown to negatively regulate RhoA activity (Yamazaki *et al*, 2009), but also to positively regulate vSMC contraction through direct phosphorylation of MLC2 (Wilson *et al*, 2005). The interaction of parvins with ILK is necessary to target both proteins to FAs and to prevent degradation of the IPP complex (Legate *et al*, 2006). However, ILK levels and localization to FAs are apparently not altered in α-pv$^{-/-}$ vSMCs. In addition, β-pv levels are upregulated in these cells, and β-pv, which also localizes to FAs, binds ILK also in the absence of α-pv. These results suggest that the β-pv upregulation acts to stabilize the IPP complex in the absence of α-pv, and is sufficient to localize this complex to FAs. However, we also show that α- and β-pv exist in separate complexes, and that the β-pv/ILK complex is unable to compensate for the loss of α-pv as a negative regulator of vSMC contractility. Furthermore, we found that depletion of ILK in wt SMA-positive cells triggers MLC2 phosphorylation accompanied by a dramatic reduction in α-pv levels, whereas the depletion of β-pv has no effect on MLC2 phosphorylation. Moreover, it has been observed that a vSMC/PCs specific-deletion of ILK leads to MCs dysfunction also associated with a RhoA-dependent hypercontractility phenotype (Kogata *et al*, 2009). This clearly indicates that ILK does not contribute to the hyperphosphorylation of MLC2 through directly phosphorylating MLC2 in α-pv$^{-/-}$ cells and that the recruitment of α-pv and ILK form a mechanosensory complex at FAs of contractile cell types such as vSMCs. This complex has an essential function in downregulating RhoA-dependent contractility to allow efficient cell spreading and migration. Consistent with our observations, a similar mechanism for ILK has been recently observed in the nervous system (Pereira *et al*, 2009). How the ILK/α-pv complex downregulates RhoA is not known. This might occur through α-pv-dependent recruitment of negative regulator(s) of the RhoA/ROCK/MLC2 signalling pathway to this complex. As we observed the RhoA downregulation only in certain cell types, the negative regulators recruited by the ILK/α-pv complex are likely to be expressed in a cell type-specific manner.

Materials and methods

Generation of α-parvin-deficient mice

A 400 bp α-parvin cDNA fragment derived from EST clone AI006605 was used to screen a 129/Sv mouse P1-derived artificial chromosome library. Five positive PAC clones were identified and used to generate the α-parvin targeting construct. To abolish α-parvin gene function, an IRES-β-galactosidase cassette and a neomycin resistance gene was inserted into exon 2. Genotyping of wt and recombinant alleles was performed by Southern blot using an external probe after PstI digestion of genomic DNA. Wt and mutant mice were genotyped by PCR using a three-primer system; forward 1 (F1) 5′-GGAATGAACGCCATCAACCT-3′, F2 5′-GATTAGATAAATGC CTGCTC-3′, reverse (R) 5′-TTGCGTGAGTTTGGATCGAC-3′.

Antibodies

The following antibodies were used: rabbit antibody against α-parvin (Chu *et al*, 2006); rabbit antibody against β-parvin (Chu *et al*, 2006); rat antibody against CD31 (PharMingen); rabbit antibody against desmin (Oldberg); Cy3-conjugated mouse antibody against αSMA (Sigma); rabbit antibody against anti-NG2 (Chemicon); mouse antibody against GAPDH (Calbiochem); rabbit antibody against ILK (Cell Signalling Technology); rabbit antibody against myosin light chain (MLC2) (Santa Cruz); rabbit antibody against phospho-MLC2 (Cell Signaling); mouse antibody against paxillin (Transduction Laboratories); Cy3-and FITC-conjugated antibodies specific for mouse IgG, rabbit IgG and rat IgG (Jackson Immunochemicals Laboratories Inc.; West Grove, PA, USA) were used as secondary antibodies. TRITC-conjugated phalloidin was used to detect F-actin (Molecular Probes; Eugene, OR, USA).

Isolation of SMA-positive cells

Embryos and YSs were harvested and washed in PBS. For each embryo, the tail was removed and used for genotyping. YSs were treated with Type I collagenase (2 mg/ml) (Invitrogen) in PBS at

37°C for 45 min. The tissue was then passed through a fine-tip Pasteur pipette with a 2-μm diameter. Cells were plated on tissue culture plates coated with 10 μg/ml FN and cultured in DMEM medium containing 10% fetal bovine serum and antibiotics. After 60 min of culture, the SMA-positive cells had attached to dish, and the medium containing visceral endoderm cells and ECs was carefully aspirated. After 2 days in culture, SMA-positive cells were used for experiments.

The same protocol was used to isolate SMA-positive cells from E9.5 embryos, which were subsequently immortalized using the SV40 T-large oncogene. SMA-positive cells were isolated and characterized by western blot and immunofluorescence analyses. To avoid changes in the contractile properties of the cells, experiments were performed with low (8–10) cell passages.

Transient expression of α-pv

α-pv-GFP was generated by cloning the murine α-pv cDNA (gift from Dr A Noegel, University of Cologne) into the pEGFP-C1 vector (Clontech). Primary cells were transiently transfected with Lipofectamine 2000 transfection reagent (Invitrogen) according to the manufacturer's protocol.

Adhesion assay

Cells (1×10^5 cells/well) were plated onto 96-well plates coated with FN, LN or collagen I. After 45 min incubation, cells were lysed in a substrate buffer (7.5 mM NPAG (Sigma), 0.1 M Na citrate pH 5, 0.5% Triton X-100) over night at 37°C. The reaction was stopped by adding 50 mM Glycine pH 10.4, 5 mM EDTA after which OD 405 was measured.

Immunoprecipitation

Cells were lysed in lysis buffer (in 150 mM NaCl, 50 mM Tris pH 8, 10 mM EDTA, 1% Triton X-100, 0,05% sodium deoxycholate supplemented with protein inhibitors (Roche) and phosphatase inhibitors (Sigma)) and 0.5 mg of cell lysate was incubated with anti-α-parvin rabbit polyclonal or anti-β-parvin rabbit polyclonal antibodies for 30 min on ice. Immunocomplexes were then bound to protein G-beads (Sigma) for 1 h, washed in lysis buffer, resuspended in SDS sample buffer (Invitrogen) and analysed by SDS–PAGE.

RhoA activation assay and affinity precipitation of cellular GTP-Rho and Rac

Freshly isolated cells from the YSs were seeded on FN (10 μg/ml) for 10 min and a quantitative assay for RhoA activity was performed using G-LISA RhoA Activation Assay Biochem Kit following the manufacturer's instructions (Cytoskeleton, Inc., CO).

For affinity precipitation of GTP-Rho and Rac, immortalized cells were lysed in lysis buffer (50 mM Tris, pH 7.4, 1% Triton X-100, 0.1% SDS, 500 mM NaCl, 10 mM $MgCl_2$, supplemented with protease inhibitors (Roche)). Cell lysates were clarified by centrifugation at 900 r.p.m. at 4°C for 10 min, and equal volumes of lysates were incubated with GST–Rhotekin (Rho) beads or GST-PAK-CRIB beads at 4°C for 60 min. The beads were washed four times with buffer B (50 mM Tris, pH 7.4, 1% Triton X-100, 150 mM NaCl, 10 mM $MgCl_2$, supplemented with protease inhibitors (Roche)). Bound Rho and Rac proteins were detected by western blotting using monoclonal antibodies against RhoA and Rac1 (Santa Cruz Biotechnology).

siRNA-mediated ILK and parvin depletions

siRNA duplexes for ILK, α-parvin, β-parvin and scrambled control were purchased from Sigma. Two siRNA duplexes (5′-CAGUGUAAU CGAUCGAUGAATT-3′ and 5′-CCAUAUGGAUCUCUCUACATT-3′ for ILK; 5′-CGACAAUGGUCGAUCCAAA-3′ and 5′-GAACAAGCAUCUGA AUAAA-3′ for α-parvin; 5′-CAAACACCUGAAUAAGCUA-3′ and 5′-CC UGACUCCUGACAGCUUU-3′ for β-parvin) were transfected into SMA-positive cells using Lipofectamine 2000 (Invitrogen) according to the manufacturer's protocol. Experiments were carried out 48 h after transfection.

SDS–PAGE and immunoblotting

Cells were lysed in lysis buffer (150 mM NaCl, 50 mM Tris pH 7,4, 1 mM EDTA, 1% Triton X-100 supplemented with protease inhibitors (Roche) and phosphatase inhibitors (Sigma)), homogenized in Laemmli sample buffer and boiled for 5 min. Cell lysates were resolved by SDS–PAGE gels. Proteins were then electrophoretically transferred from gels onto nitrocellulose membranes, followed by incubation with antibodies. Bound antibodies were detected using enhanced chemiluminescence (Millipore Corporation, Billerica, USA).

Whole embryo immunohistochemistry

Staged embryos were dissected in PBS and genotyped by PCR. YSs and embryos were fixed overnight in fixation buffer (80% methanol, 20% DMSO). Samples were rehydrated in 0.1% Tween-20 in PBS, incubated in blocking buffer (10% goat serum, 5% BSA in PBS) for 2 h, and exposed to primary antibody overnight at 4°C. After 5–7 h wash with 0.1% Tween-20 in PBS, samples were incubated with secondary antibodies overnight at 4°C.

Histology of tissue sections, immunostaining and morphological analysis

Immunohistochemistry and immunofluorescence studies of embryos, YSs and cells were performed as described earlier in Montanez *et al* (2008). Analysis of vessel diameter was performed as described by Grazioli *et al* (2006). Three embryos of each genotype were analysed. The area and the shape factor (4πarea/perimeter^2) of cells were analysed using the MetaMorph software. The data represent three independent assays (150 cells/experiment).

Migration assay

Chemotactic and chemokinetic migration assays were performed in 3-μm pore size chamber inserts (BD Falcon). For chemotaxis assays, 4×10^4 cells were plated into the chamber and transferred into 24-well plates containing serum-free medium with or without 20 ng/ml PDGF-BB. For chemokinesis assays, 4×10^4 cells in serum-free medium with or without 20 ng/ml PDGF-BB were plated into the chamber and transferred into 24-well plates containing serum-free medium.

After overnight incubation, the cells in the bottom part of the chamber were stained with a crystal violet solution and counted. Five microscopic fields per chamber were analysed. Data are represented as percentage of total cell number/field ± s.d. The assay was performed in triplicate in three independent assays.

Collagen matrix contraction assay

Cells were suspended in a collagen mixture (1.6 mg/ml collagen I (INAMED), 7.5% NaHCO3 in cell culture medium (MEM)) with a final concentration of 4×10^5 cells/ml. A measure of 100 μl of the collagen-cell mixture was placed in a 24-well suspension culture plate (Greiner) and incubated for 1 h under standard cell culture conditions causing the polymerization of the collagen. Finally, 2 ml of cell culture medium (DMEM + 10% serum) was applied on top of the gel. The area of the collagen lattices was calculated after 24 and 48 h of culture. The assay was performed in triplicate in three independent assays.

Statistical analysis

The statistical analysis was performed using the Mann–Whitney test. The values are presented as mean + s.e.m. At least three independent experiments were performed.

Supplementary data

Supplementary data are available at *The EMBO Journal* Online (http://www.embojournal.org).

Acknowledgements

We thank Simone Bach for expert technical assistance, Michela Carlet for initial parvin immunoprecipitations, Dr Angelika A Noegel (University of Cologne, Germany) for α-pv cDNA, and Drs Roy Zent, Kyle Legate and Markus Moser for carefully reading the manuscript. This work was supported by the Sigrid Juselius Foundation, the Finnish Cultural Foundation, and the Academy of Finland (to SAW), the Austrian Science Funds (SFB021) and by the Max Planck Society (to RF).

Conflict of interest

The authors declare that they have no conflict of interest.

References

Abraham S, Kogata N, Fässler R, Adams RH (2008) Integrin beta1 subunit controls mural cell adhesion, spreading, and blood vessel wall stability. *Circ Res* **102:** 562–570

Abramsson A, Kurup S, Busse M, Yamada S, Lindblom P, Schallmeiner E, Stenzel D, Sauvaget D, Ledin J, Ringvall M, Landegren U, Kjellén L, Bondjers G, Li JP, Lindahl U, Spillmann D, Betsholtz C, Gerhardt H (2007) Defective N-sulfation of heparan sulfate proteoglycans limits PDGF-BB binding and pericyte recruitment in vascular development. *Genes Dev* **21:** 316–331

Adamo L, Naveiras O, Wenzel PL, McKinney-Freeman S, Mack PJ, Gracia-Sancho J, Suchy-Dicey A, Yoshimoto M, Lensch MW, Yoder MC, García-Cardeña G, Daley G (2009) Biochemical forces promote embryonic hematopiesis. *Nature* **459:** 1068–1069

Adams RH, Alitalo K (2007) Molecular regulation of angiogenesis and lymphangiogenesis. *Nat Rev Mol Cell Biol* **8:** 464–478

Amano M, Ito M, Kimura K, Fukata Y, Chihara K, Nakano T, Matsuura Y, Kaibuchi K (1996) Phosphorylation and activation of myosin by Rho-associated kinase (Rho-kinase). *J Biol Chem* **271:** 20246–20249

Arthur WT, Petch LA, Burridge K (2000) Integrin engagement suppresses RhoA activity via a c-Src-dependent mechanism. *Curr Biol* **10:** 719–722

Arthur WT, Burridge K (2001) RhoA inactivation by p190RhoGAP regulates cell spreading and migration by promoting membrane protrusion and polarity. *Mol Biol Cell* **12:** 2711–2720

Beck Jr L, D'Amore PA (1997) Vascular development: cellular and molecular regulation. *FASEB J* **11:** 365–373

Bendig G, Grimmler M, Huttner IG, Wessels G, Dahme T, Just S, Trano N, Katus HA, Fishman MC, Rottbauer W (2006) Integrin-linked kinase, a novel component of the cardiac mechanical stretch sensor, controls contractility in the zebrafish heart. *Genes Dev* **20:** 2361–2372

Boucher P, Gotthardt M, Li WP, Anderson RG, Herz J (2003) LRP: role in vascular wall integrity and protection from atherosclerosis. *Science* **300:** 329–332

Burridge K, Wennerberg K (2004) Rho and Rac take center stage. *Cell* **116:** 167–179

Carlson TR, Hu H, Braren R, Kim YH, Wang RA (2008) Cell-autonomous requirement for beta1 integrin in endothelial cell adhesion, migration and survival during angiogenesis in mice. *Development* **135:** 2193–2202

Chen H, Huang XN, Yan W, Chen K, Guo L, Tummalapali L, Dedhar S, St-Arnaud R, Wu C, Sepulveda JL (2005) Role of the integrin-linked kinase/PINCH1/alpha-parvin complex in cardiac myocyte hypertrophy. *Lab Invest* **85:** 1342–1356

Chu H, Thievessen I, Sixt M, Lämmermann T, Waisman A, Braun A, Noegel AA, Fässler R (2006) Gamma-Parvin is dispensable for hematopoiesis, leukocyte trafficking, and T-cell-dependent antibody response. *Mol Cell Biol* **26:** 1817–1825

Cramer LP, Mitchison TJ (1995) Myosin is involved in postmitotic cell spreading. *J Cell Biol* **131:** 179–189

Danen EH, van Rheenen J, Franken W, Huveneers S, Sonneveld P, Jalink K, Sonnenberg A (2005) Integrins control motile strategy through a Rho-cofilin pathway. *J Cell Biol* **169:** 515–526

del Pozo MA, Price LS, Alderson NB, Ren XD, Schwartz MA (2000) Adhesion to the extracellular matrix regulates the coupling of the small GTPase Rac to its effector PAK. *EMBO J* **19:** 2008–2014

Fässler R, Rohwedel J, Maltsev V, Bloch W, Lentini S, Guan K, Gullberg D, Hescheler J, Addicks K, Wobus AM (1996) Differentiation and integrity of cardiac muscle cells are impaired in the absence of beta 1 integrin. *J Cell Sci* **109:** 2989–2999

Friedrich EB, Liu E, Sinha S, Cook S, Milstone DS, MacRae CA, Mariotti M, Kuhlencordt PJ, Force T, Rosenzweig A, St-Arnaud R, Dedhar S, Gerszten RE (2004) Integrin-linked kinase regulates endothelial cell survival and vascular development. *Mol Cell Biol* **24**: 8134–8144

George EL, Georges-Labouesse EN, Patel-King RS, Rayburn H, Hynes RO (1993) Defects in mesoderm, neural tube and vascular development in mouse embryos lacking fibronectin. *Development* **119:** 1079–1091

Grazioli A, Alves CS, Konstantopoulos K, Yang JT (2006) Defective blood vessel development and pericyte/pvSMC distribution in alpha 4 integrin-deficient mouse embryos. *Dev Biol* **293:** 165–177

Hellström M, Kalén M, Lindahl P, Abramsson A, Betsholtz C (1999) Role of PDGF-B and PDGFR-beta in recruitment of vascular smooth muscle cells and pericytes during embryonic blood vessel formation in the mouse. *Development* **126:** 3047–3055

Hellström M, Gerhardt H, Kalén M, Li X, Eriksson U, Wolburg H, Betsholtz C (2001) Lack of pericytes leads to endothelial hyperplasia and abnormal vascular morphogenesis. *J Cell Biol* **153:** 543–553

Huang C, Sheikh F, Hollander M, Cai C, Becker D, Chu PH, Evans S, Chen J (2003) Embryonic atrial function is essential for mouse embryogenesis, cardiac morphogenesis and angiogenesis. *Development* **130:** 6111–6119

Hynes RO (2002) Integrins: bidirectional, allosteric signaling machines. *Cell* **110:** 673–687

Karnam SM (2006) Signaling for contraction and relaxation in smooth muscle of the gut. *Annu Rev Physiol* **68:** 345–374

Kimura K, Ito M, Amano M, Chihara K, Fukata Y, Nakafuku M, Yamamori B, Feng J, Nakano T, Okawa K, Iwamatsu A, Kaibuchi K (1996) Regulation of myosin phosphatase by Rho and Rho-associated kinase (Rho-kinase). *Science* **273:** 245–248

Kogata N, Tribe RM, Fassler R, Way M, Adams RH (2009). Integrin-linked kinase controls vascular wall formation by negatively regulating Rho/ROCK-mediated vascular smooth muscle cell contraction. *Genes Dev* (in press)

LaLonde DP, Grubinger M, Lamarche-Vane N, Turner CE (2006) CdGAP associates with actopaxin toregulate integrin-dependent changes in cell morphology and motility. *Curr Biol* **16:** 1375–1385

Legate KR, Montañez E, Kudlacek O, Fässler R (2006) ILK, PINCH and parvin: the tIPP of integrin signalling. *Nat Rev Mol Cell Biol* **7:** 20–31

Legate KR, Wickström SA, Fässler R (2009) Genetic and cell biological analysis of integrin outside-in signaling. *Genes Dev* **23:** 397–418

Lucitti JL, Jones EA, Huang C, Chen J, Fraser SE, Dickinson ME (2007) Vascular remodeling of the mouse yolk sac requires hemodynamic force. *Development* **134:** 3317–3326

Matsumura F, Hartshorne DJ (2008) Myosin phosphatase target subunit: many roles in cell function. *Biochem Biophys Res Commun* **369**: 149–156

Montanez E, Ussar S, Schifferer M, Bösl M, Zent R, Moser M, Fässler R (2008) Kindlin-2 controls bidirectional signaling of integrins. *Genes Dev* **22:** 1325–1330

Nikolopoulos SN, Turner CE (2000) Actopaxin, a new focal adhesion protein that binds paxillin LD motifs and actin and regulates cell adhesion. *J Cell Biol* **151:** 1435–1448

North TE, Goessling W, Peeters M, Li P, Ceol C, Lord AM, Weber GJ, Harris J, Cutting CC, Huang P, Dzierzak E, Zon LI (2009) Hematopoietic stem cell development is dependent on blood flow. *Cell* **137:** 736–748

Olski TM, Noegel AA, Korenbaum E (2001) Parvin, a 42 kDa focal adhesion protein, related to the alpha-actinin superfamily. *J Cell Sci* **114:** 525–538

Pereira JA, Benninger Y, Baumann R, Gonçalves AF, Ozçelik M, Thurnherr T, Tricaud N, Meijer D, Fässler R, Suter U, Relvas JB (2009) Integrin-linked kinase is required for radial sorting of axons and Schwann cell remyelination in the peripheral nervous system. *J Cell Biol* **185:** 147–161

Pöschl E, Schlötzer-Schrehardt U, Brachvogel B, Saito K, Ninomiya Y, Mayer U (2004) Collagen IV is essential for basement membrane stability but dispensable for initiation of its assembly during early development. *Development* **131:** 1619–1628

Ren XD, Kiosses WB, Schwartz MA (1999) Regulation of the small GTP-binding protein Rho by cell adhesion and the cytoskeleton. *EMBO J* **18:** 578–585

Ridley AJ, Schwartz MA, Burridge K, Firtel RA, Ginsberg MH, Borisy G, Parsons JT, Horwitz AR (2003) Cell migration: integrating signals from front to back. *Science* **302:** 1704–1709

Risau W (1997) Mechanism of angiogenesis. *Nature* **386:** 671–674

Sander EE, ten Klooster JP, van Delft S, van der Kammen RA, Collard JG (1999) Rac downregulates Rho activity: reciprocal balance between both GTPases determines cellular morphology and migratory behavior. *J Cell Biol* **147:** 1009–1022

Sengbusch JK, He W, Pinco KA, Yang JT (2002) Dual functions of [alpha]4[beta]1 integrin in epicardial development: initial migration and long-term attachment. *J Cell Biol* **157:** 873–882

Tanjore H, Zeisberg EM, Gerami-Naini B, Kalluri R (2008) Beta1 integrin expression on endothelial cells is required for angiogenesis but not for vasculogenesis. *Dev Dyn* **237:** 75–82

Thyboll J, Kortesmaa J, Cao R, Soininen R, Wang L, Iivanainen A, Sorokin L, Risling M, Cao Y, Tryggvason K (2002) Deletion of the laminin alpha4 chain leads to impaired microvessel maturation. *Mol Cell Biol* **22:** 1194–1202

Tsuji T, Ishizaki T, Okamoto M, Higashida C, Kimura K, Furuyashiki T, Arakawa Y, Birge RB, Nakamoto T, Hirai H, Narumiya S (2002) ROCK and mDia1 antagonize in Rho-dependent Rac activation in Swiss 3T3 fibroblasts. *J Cell Biol* **157:** 819–830

Tu Y, Huang Y, Zhang Y, Hua Y, Wu C (2001) A new focal adhesion protein that interacts with integrin-linked kinase and regulates cell adhesion and spreading. *J Cell Biol* **153:** 585–598

Wilson DP, Sutherland C, Borman MA, Deng JT, Macdonald JA, Walsh MP (2005) Integrin-linked kinase is responsible for Ca2 + -independent myosin diphosphorylation and contraction of vascular smooth muscle. *Biochem J* **392:** 641–648

Worthylake RA, Burridge K (2003) RhoA and ROCK promote migration by limiting membrane protrusions. *J Biol Chem* **278:** 13578–13584

Xu J, Wang F, Van Keymeulen A, Herzmark P, Straight A, Nelly K, Takuwa Y, Sugimoto N, Mitchison T, Bourne HR (2003) Divergent signals and cytoskeletal assemblies regulate self-organizing polarity in neutrophils. *Cell* **114:** 201–214

Yamaji S, Suzuki A, Sugiyama Y, Koide Y, Yoshida M, Kanamori H, Mohri H, Ohno S, Ishigatsubo Y (2001) A novel integrin-linked kinase-binding protein, affixin, is involved in the early stage of cell-substrate interaction. *J Cell Biol* **153:** 1251–1264

Yamazaki T, Masuda J, Omori T, Usui R, Akiyama H, Maru Y (2009) EphA1 interacts with integrin-linked kinase and regulates cell morphology and motility. *J Cell Sci* **122:** 243–255

